SUPPORTING INFORMATION

Journal: **ENVIRONMENTAL SCIENCE & TECHNOLOGY**

Date: 24/07/2009

MS No.: es-2009-01399q

Pages: 19

Figures: 12

Tables: 2

Fate of Silica Nanoparticles in Simulated Primary Wastewater Treatment

Helen P. Jarvie[1], Hisham Al-Obaidi[2], Stephen M. King[3], Michael J. Bowes[1], M. Jayne Lawrence[2], Alex F. Drake[2], Mark A. Green[4] and Peter J. Dobson[5]

[1] NERC Centre for Ecology and Hydrology, Maclean Building, Benson Lane, Crowmarsh Gifford, Wallingford OX10 8BB, UK

[2] School of Biomedical and Health Sciences, King's College London, Franklin-Wilkins Building, Stamford Street, London SE1 9NH, UK

[3] STFC ISIS Facility, Rutherford Appleton Laboratory, Harwell Science & Innovation Campus, Didcot OX11 0QX, UK

[4] Department of Physics, King's College London, Strand, London WC2R 2LS, UK

[5] Department of Engineering Science, University of Oxford, Parks Road, Oxford OX1 3PJ, UK

1. Supplementary Figures

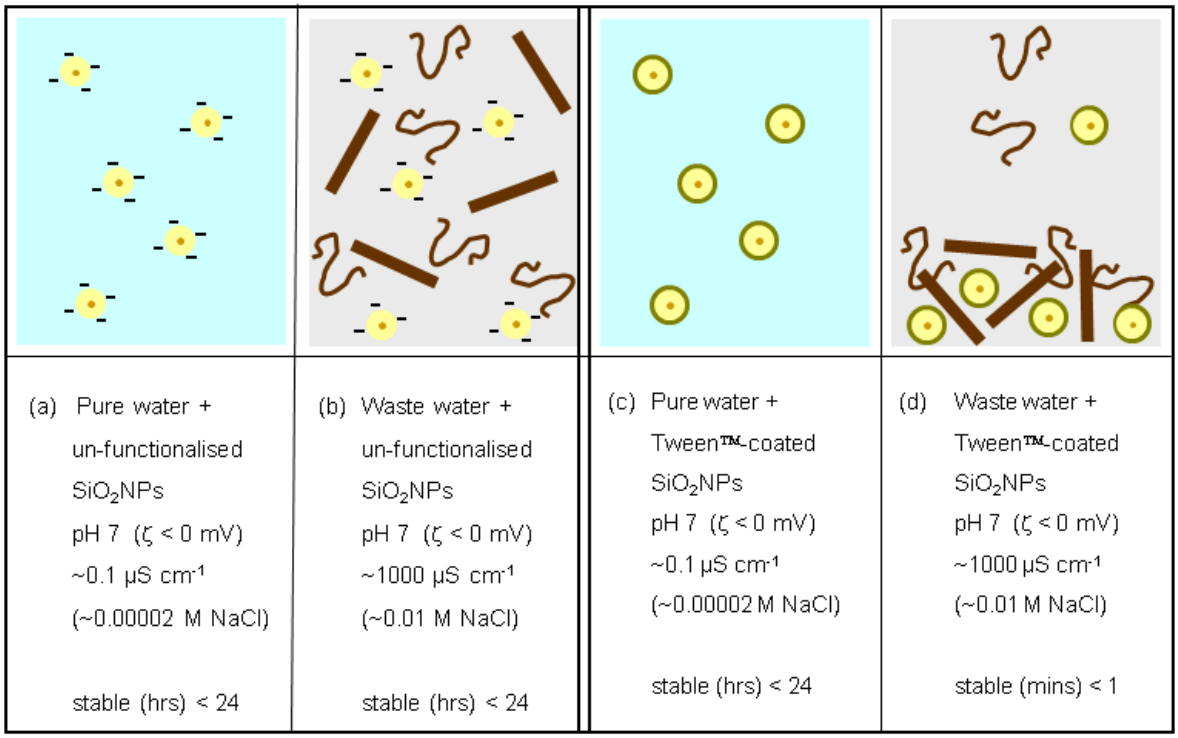

Figure SI-1 Schematic Summary of the Fate of Functionalised and Surfactant-coated Silica Nanoparticles (SiO_2NPs). The figure depicts the unfunctionalised and Tween^{TM}-coated core-shell SiO_2NPs in both pure water (blue) and wastewater (grey). The wastewater contains a variety of organic matter from macroscopic fibres to natural polymers (brown).

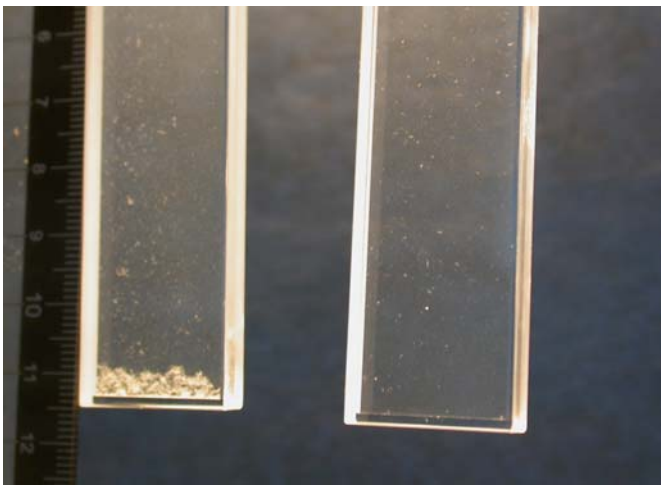

Figure SI-2 Effect of Wastewater Screening. Key: (left) raw wastewater (as collected); (right) 'screened' wastewater (after screening through glass wool to remove larger particulates)

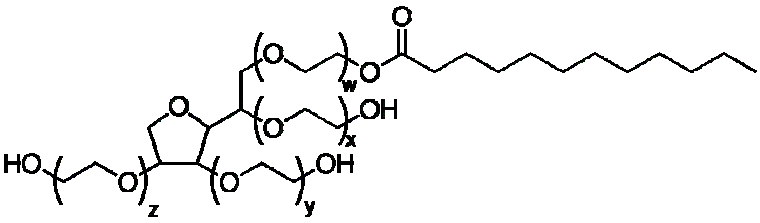

Figure SI-3 Chemical Structure of Tween™ 20 (Polysorbate™ 20). w+x+y+z=20.

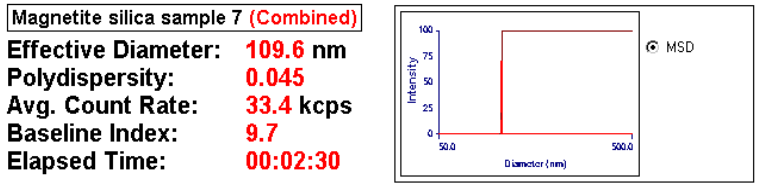

Magnetite silica sample 7 (Combined)

Effective Diameter: 109.6 nm
Polydispersity: 0.045
Avg. Count Rate: 33.4 kcps
Baseline Index: 9.7
Elapsed Time: 00:02:30

MSD

Run	Eff. Diam. (nm)	Half Width (nm)	Polydispersity	Baseline Index
1	113.1	8.0	0.005	7.9
2	111.2	7.9	0.005	6.5
3	109.5	26.9	0.060	9.1
4	110.0	13.5	0.015	9.8
5	104.5	37.5	0.128	7.4
Mean	109.7	18.7	0.043	8.1
Std. Error	1.4	5.8	0.024	0.6
Combined	109.6	23.4	0.045	9.7

Figure SI-4 Representative SiO_2NP Particle Size Data. From dynamic light scattering at 90°.

Figure SI-5 Long-term Stability of the SiO_2NP Dispersions. Unfunctionalised SiO_2NPs dispersed in nanopure water after approximately 80 hours.

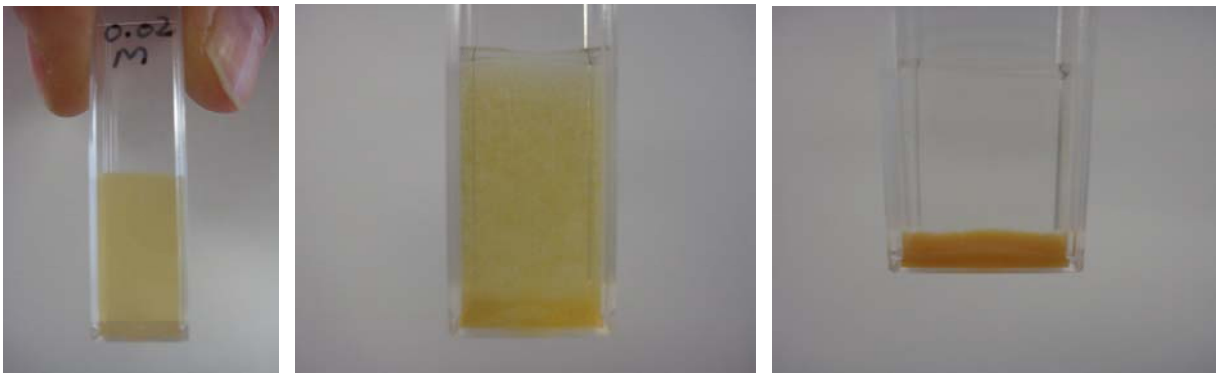

Figure SI-6 Colloidal Stability of the Unfunctionalised SiO_2NP Dispersions. Key: Unfunctionalised SiO_2NPs dispersed in 0.01 M $La(NO_3)_3$ after (left) 7 minutes, (centre) 9 minutes and (right) 35 minutes. Note that the label on the cuvette in the first image refers to the initial electrolyte concentration before 1:1 dilution with the nanoparticle dispersion.

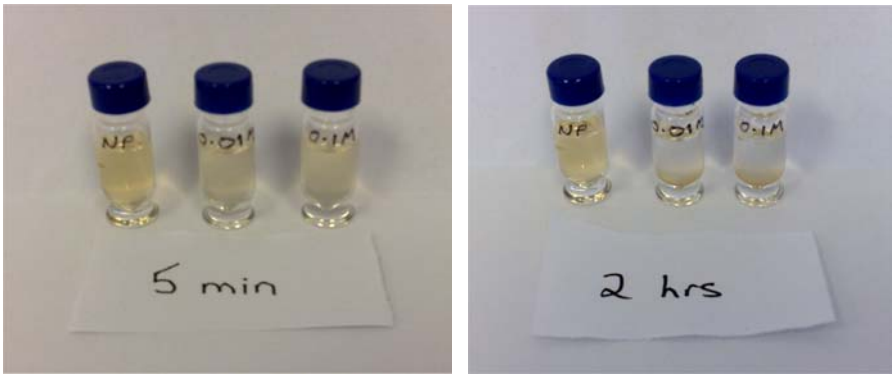

Figure SI-7 Colloidal Stability of Tween™-coated SiO_2NP Dispersions. Key: Tween™-coated SiO_2NPs dispersed in (L-R) nanopure water, 0.01 M $La(NO_3)_3$ and 0.10 M $La(NO_3)_3$ after (left) 5 minutes and (right) 2 hours.

Figure SI-8 Sample Cuvette.

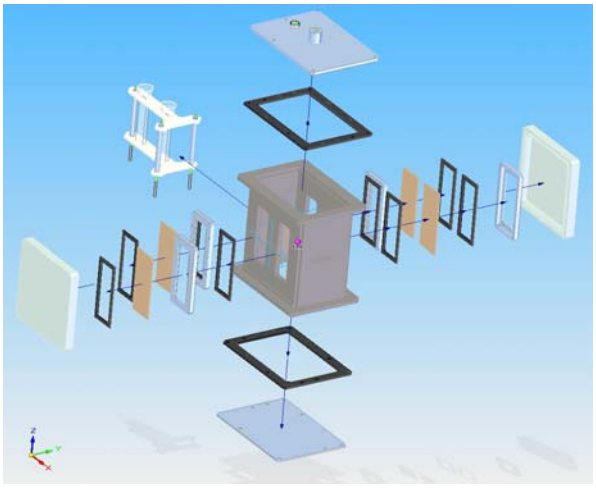

Figure SI-9 Biological Containment Vessel (BCV). Exploded view showing neutron windows, protective Perspex transportation window covers and seals.

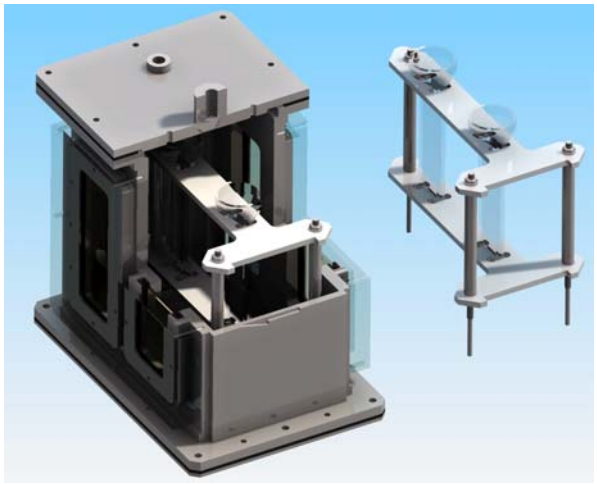

Figure SI-10 Biological Containment Vessel (BCV). 3D cut-away view showing the PTFE sample carriage holding two cuvettes.

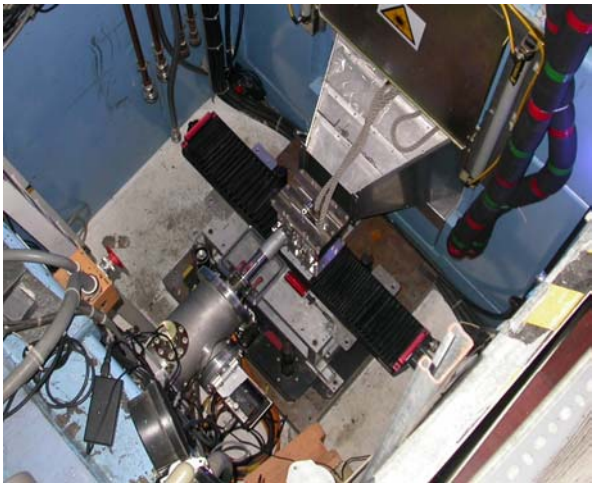

Figure SI-11 LOQ Instrument Sample Position. View after BCV installation onto the horizontal and vertical motion stages. The neutrons exit the ‘pipe’ in the centre of the image.

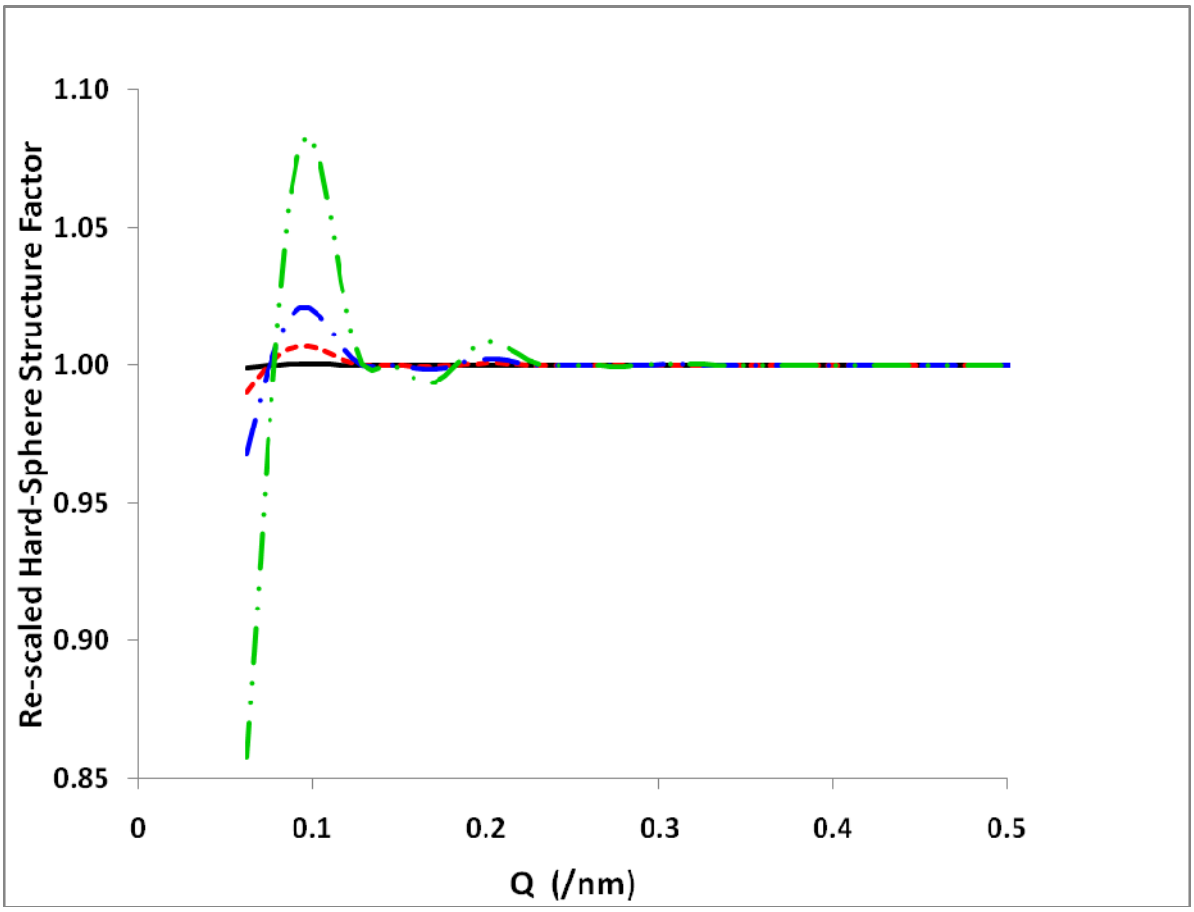

Figure SI-12 Hard-sphere structure factors. Calculated data for 60 nm diameter spherical particles at different concentrations: (black, continuous line) 0.09 $\%^{v}/_{v}$, as used in SANS experiments; (red, dotted line) 1 $\%^{v}/_{v}$; (blue, chain dashed line) 3 $\%^{v}/_{v}$; (green, double chain dashed line) 10 $\%^{v}/_{v}$.

2. Methods

2.1 Wastewater

Raw (untreated) wastewater was sourced from the inlet stream of a Wastewater Treatment Works in South East England serving a semi-urban area of approximately 297,000 population equivalents, immediately after screening and grit removal (which excludes debris >5mm), but before primary treatment (5 circular clarifier tanks of diameter 42.8 m). The dry weather flow to works is c. 60,000 m^3

day^{-1}, whilst the maximum design flow to works is 3.8 × {dry weather flow}. The flow to works during wastewater sample collection (Wednesday 9th July 2008 at 10:45 BST) was 74,476 m^3 day^{-1}. The hydraulic retention time is estimated at c. 2 hours with a hydraulic loading of c. 30 – 45 m^3 m^{-2} day^{-1}.

Wastewater samples were immediately refrigerated prior to use, to minimise sample degradation, and all experiments were performed within 48 hours of collection. Aliquots of the untreated wastewater were screened under gravity through a glass wool plug to remove the larger debris and other detritus with length scales in the order of millimeters. See Figure SI-2.

2.2 Wastewater Characteristics

The pH of the raw wastewater was 7.18, and the conductivity 920 μS cm^{-1}. The total suspended solids concentration was 293 mg L^{-1}, equivalent to a suspended solids loading of 22 tonnes day^{-1}.

The results of background chemical analyses are presented in Table SI-1, where they are also compared with 'typical' values of domestic raw wastewater from other studies.

2.3 Nanoparticle Synthesis

Fe_3O_4-cored silica nanoparticles were prepared by a variation of a methodology described previously *(1,2)*. Briefly, $FeCl_2$ (2.08 g) and $FeCl_3$ (5.22 g) were dissolved in deionised water (380 mL) and ammonium hydroxide (20 mL) added. A magnet was used to separate the resultant precipitate and the supernatant was discarded by decantation. 2 M HNO_3 (40 mL) and 0.35M $Fe(NO_3)_3$ (60 mL) were added to the precipitate and the suspension was left to boil for 90 minutes. The brown precipitate thus formed was washed with 2M HNO_3 (total 500 mL) and re-dispersed in deionised water (1 L). Sufficient 0.01 M citric acid solution was added to 45 mL of the re-dispersed nanoparticles until flocculation was

observed (pH~3). Tetramethylammonium hydroxide (maximum 10 mL) was then gradually added to obtain a final dispersion pH of 7 and redisperse the nanoparticles.

These citric acid-coated magnetite nanoparticles were then coated with silica by the following process. First 45 mL absolute ethanol, 20 mL water and 1 mL (30%) ammonium hydroxide solution were added to 1 mL of Fe_3O_4 nanoparticle suspension. The suspension was stirred and 0.15 mL tetraethylorthosilane added, then left stirring for 24 hours. The resulting suspension of silica-coated Fe_3O_4 nanoparticles (SiO_2NPs) was stored in a fridge (4 °C) until needed.

Before use the SiO_2NPs were first exchanged into absolute ethanol by centrifugation (13000 rpm for 5 minutes) and resuspension. This procedure was repeated before the SiO_2NPs were finally resuspended into deionised water and ensured that the final pH of the suspension was close to 7. These unfunctionalised SiO_2NPs at 0.02% $^{v}/_{v}$ were indefinitely stable in deionised water (Figure SI-5).

2.4 Nanoparticle Functionalisation

To functionalise the SiO_2NPs, the washed suspension was concentrated by centrifugation and resuspended into a dilute solution (0.01%$^{w}/_{v}$) of the pharmaceutical-grade non-ionic surfactant Tween™ 20 (Polysorbate™ 20, Figure SI-3). This concentration is approximately equivalent to the critical micelle concentration (CMC ~8×10^{-5} M) *(3)*. The surfactant molecules physically adsorb at the particle surface through Van der Waals interactions. The surfactant-coated SiO_2NPs were checked by light scattering after functionalisation. No aggregation was observed.

The adsorbtion of non-ionic surfactants onto silica from aqueous solution has been widely studied and is quite complex, being a balance between hydrophilic and hydrophobic interactions both in solution and at the silica surface *(4)*. The structurally-related polyoxyethylene monoalkylether (Brij™) surfactants form a surface bilayer structure - silica-(oxyethylene 'head'-alkyl 'tail')-(alkyl 'tail'-oxyethylene

'head') when adsorbing from micellar solution, giving adsorbed amounts between 5 - 9 μmol/m^2 *(5)*. We assume Tween™ 20 would adsorb in a similar manner but calculate that our adsorbed amounts would only be around 2 – 3 μmol/m^2 (see below). This suggests that most of the Tween™ molecules added to the SiO_2NP dispersion adsorb, but that that the particles are unlikely to be completely covered in surfactant.

2.5 Nanoparticle Characterisation

Light Scattering

Particle size measurements were routinely performed using a Brookhaven ZetaPlus (Brookhaven Instruments Corporation, USA) dynamic light scattering instrument operating at a laser wavelength of 677 nm and a fixed scattering angle of 90°. The refractive index used was 1.33 and the viscosity input was 0.89 cP. Particle shape and/or polydispersity in particle size was checked by investigating the angular variation of both the size and scattered light using an ALV-5000 (ALV-Laser Vertriebsgesellschaft mbH Lagen, Germany) multi-tau dynamic light scattering apparatus *in static mode*. Measurements were performed at a laser wavelength of 633 nm over a scattering angle range of 30-150°. Toluene was used as a reference scatterer. To reduce the effects of multiple scattering in these measurements, the prepared SiO_2NP suspension was diluted with filtered deionised water to a particle concentration of approximately 0.001 $\%^{v}/_{v}$. Typical particle size data from the two methods are shown in Figure SI-4 and Table SI-2.

Transmission electron microscope (TEM)

The morphology of the synthesised SiO_2NPs was observed with a Philips Tecnai-12 FEI Transmission Electron Microscope (TEM) using an accelerating voltage of 120 kV. The TEM samples were prepared

by depositing a drop of SiO_2NP suspension on a carbon-coated copper grid and evaporating the liquid for 5-10 minutes prior to examination in the microscope. A typical micrograph is shown in Figure 1 in the main text.

Both light scattering and TEM show the SiO_2NPs to have an extremely narrow size distribution, although there is some disagreement over the actual size. Light scattering suggests a mean diameter of 110 ±17% nm, whilst TEM suggests something nearer 65 nm. This is in fact a widely-reported phenomenon, variously attributed to hydration shells, shrinkage in a vacuum (TEM), and differential swelling *(6)*. Furthermore in the case of Fe_3O_4 colloids, absorbtion of light (due to their colour) and perturbations to normal Van der Waals interactions (from magnetic coupling) have also been shown to have an effect *(7)*. For comparison, the SiO_2NP diameters derived from applying equations SI-2 and SI-4 to the SANS data were 56±22% nm. While these are consistent with the TEM and light scattering results, the SANS data will also be a slight under-estimate because of the inhomogeneous nature of the SiO_2NPs. However, all size information derived from the SANS measurements alone will be internally consistent.

2.6 Neutron Scattering Sample Containment

The wastewater samples were contained in custom-fabricated, rectangular, Suprasil™ synthetic quartz cuvettes (Starna Scientific, Hainault, UK) of 2 mm path length and fitted with GL14 screw caps (Figure SI-8). The capacity of each cuvette was 4 ml. Synthetic quartz was chosen because it is essentially transparent to long wavelength neutrons. It may also be readily disinfected, cleaned, and autoclaved.

However, a risk assessment of the biological hazards posed by the raw wastewater, coupled with the fragility of the cuvettes, determined that, by law, sample handling would need to be conducted according to Containment Level 2 protocols. For this reason filled cuvettes were transported and measured inside leakproof Biological Containment Vessels (BCV) of in-house design (ISIS, UK)

(Figures SI-9 & SI-10). Each BCV could take two cuvettes held firmly in a PTFE sample carriage. The BCV's were fabricated in stainless steel with demountable end plates and 2 mm thick Suprasil™ quartz beam entry and exit windows. During carriage and installation the quartz windows were protected by substantial Perspex covers. The total mass of a loaded BCV was approximately 10 kg. Engineering drawings for the BCV's are available on request from S.M.K.

2.7 SANS Measurements

Whilst hydrogenous matrices are not normally considered optimal in SANS experiments (because of the large incoherent scattering cross-section of ^{1}H), they may, nonetheless, be employed provided the neutron path length is kept short and there is strong neutron scattering length density difference (or 'contrast') between the SiO_2NPs and the aqueous matrix (see Data Analysis below).

LOQ *(8)* is a fixed-geometry, 'white beam', SANS instrument that uses time-of-flight techniques on neutron wavelengths between $0.22 \leq \lambda \leq 1.0$ nm to provide a continuous and simultaneous scattering vector range of $0.06 \leq Q \leq 14$ nm^{-1}. The data were reduced according to standard procedures *(9)*. These treated data were then placed on an absolute intensity scale by comparison with the scattering from a well-characterised polymer calibration standard *(10)* measured with the same instrument configuration. The scattering from nanopure water, unscreened wastewater, and screened wastewater were each measured for background correction purposes. Data were collected in approximately 30 minute intervals over periods of 2 - 3 hours per sample.

The BCV was mounted on top of a computer-controlled horizontal translation stage, itself sat on top of a computer-controlled vertical height stage (Figure SI-11). Thus it was possible to remotely scan the height of either sample cuvette. The neutron beam was collimated to a rectangle 15 (W) x 8 (H) mm immediately before the BCV beam entry window. To look for sedimentation or flocculation effects, measurements were made at two positions: one 5 mm above, and the other 68 mm above, the bottom of

the cuvettes (the distances refer to the centre of the beam aperture). The lower measurement position was located just above the sedimented material. Indeed, the absence of any significant increase in SiO_2NP concentrations with time at the lower measurement position (Table 1, main text) confirmed that the lower measurement position was suitably located above the layer of sedimented material.

Transmissions and the background measurements were performed 53 mm above the bottom of the cuvettes (i.e., in-between the other positions). Measurements were performed at ambient temperature (*circa* 23 °C, July 10-11 2008). It should be noted that the BCV's constituted a significant thermal mass and so the temperature of the samples is unlikely to have varied greatly.

2.8 Neutron Scattering Length Density

The neutron scattering length density ρ is given by:

$$\rho = \frac{\delta \cdot N_A \cdot \sum_{i=1}^{n} b_i}{M} \qquad \text{(SI-1)}$$

where δ is the macroscopic bulk density of the molecule, M is its molecular weight, b_i is the coherent nuclear scattering length of atom i, and the summation extends over all atoms in the molecule. Values of b for the various elements may be found in standard tables or on the world-wide web. The approximate volume composition of the SiO_2NPs used in this work was 20:80 Fe_3O_4:SiO_2 for which $\rho_{NP} \sim +4.19\times10^{10}$ cm^{-2} for δ =2.8 g cm^{-3}. This is actually higher than the value for silica alone, $\rho_{SiO2} \sim +3.47\times10^{10}$ cm^{-2}, and was part of the rationale for using the engineered nanoparticles. As $\rho_{H2O} \sim -0.55\times10^{10}$ cm^{-2} it can be seen that the SiO_2NPs had good contrast against the background matrix.

2.9 Data Analysis

The treated data were modelled with two different scattering laws: that for homogeneous spherical objects of radius R given by

$$F(Q,R)_{sphere} = \frac{4\pi.R^3}{3}\left[\frac{3\,.\,(\sin(Q.R) - Q.R\,.\,\cos(Q.R))}{(Q.R)^3}\right]^2 \qquad \text{(SI-2)}$$

convoluted with a Schultz particle size distribution *(11)*, and that for surface fractals of surface fractal dimension D_s and fractal 'cut-off' length l given by

$$F(Q,R,l,D_s)_{surface\ fractal} = F(Q,R)_{sphere}\,.\,S(Q,l,D_s)_{surface\ fractal} \qquad \text{(SI-3)}$$

where one widely used *S(Q)* function is *(12,13)*

$$S(Q,l,D_s)_{surface\ fractal} = [(\Gamma(5-D_s)\,.\,l^{(5-D_s)}\,.\,[1+(Q^2.\,l^2)]^{(D_s-5)/2}\,.\,\sin[(D_s-5)\,.\,\arctan(Q\,.\,l)])\,/\,Q] \qquad \text{(SI-4)}$$

As *S(Q)* only describes the fractal structure, and not the shape or size of the elements from which that structure is constituted, it is necessary to multiply it by a function representative of the shape of the constituents. Here, for obvious reasons, we have assumed this to be spherical and have used Equation SI-4 with R set at the value obtained from the application of model (a) alone. *Γ(x)* is the Gamma function.

D_s manifests itself on *I(Q)* as a power law region in Q, that is

$$I(Q) \propto Q^{-n} \qquad \text{(SI-5)}$$

where *(14)*

$$n = 2.D_m - D_s \qquad \text{(SI-6)}$$

If $n \leq 3$ then the scattering objects are mass fractals, whereas if $n > 3$ they are surface fractals. From this it follows that in a mass fractal system $D_m \leq 3$, and in a surface fractal system $2 < D_s < 3$ (if the interface is smooth then $D_s = 2$).

Typically, in our work, $l \sim 100$ nm and so the power law region was concentrated at smaller values of Q.

The *Tween*^{TM}*-coated* nanoparticles were modelled with an additional scattering law, that of a homogenous sphere of radius *R* surrounded by an outer shell of thickness *t*:

$$I(Q) = K \,.\, N \,.\, F(Q) + B \qquad \text{(SI-7)}$$

$$F(Q,R,t)_{core-shell} = \frac{16\pi^2}{9}\Big[(\rho_{core} - \rho_{shell})^2 \,.\, R_{core}^6 \,.\, F(Q,R_{core})_{sphere} + (\rho_{shell} - \rho_{H2O})^2 \,.\, (R_{core}+t)^6 \,.\, F(Q,R_{core}+t)_{sphere} +\Big]$$

$$\Big[+\,2\,.\,(\rho_{shell} - \rho_{H2O})\,.\,(\rho_{core} - \rho_{shell})\,.\,R_{core}^3 \,.\, (R_{core}+t)^3 \,.\, f(Q,R_{core})\,.\, f(Q,R_{core}+t)\Big] \qquad \text{(SI-8)}$$

where

$$f(Q,R) = \left[\frac{3\,.\,(\sin(Q.R) - Q.R\,.\cos(Q.R))}{(Q.R)^3}\right] \qquad \text{(SI-9)}$$

In all cases it was found that the SANS data could be quite adequately modeled *without* invoking an additional inter-particle pair potential contribution. In essence, at the volume fraction of nanoparticles studied, inter-particle interactions are so long-range and so weak that they can be reasonably ignored. This is illustrated in Figure SI-12 by the absence of any prominent correlation peaks in the calculated inter-particle structure factors for volume fractions < 3%. The calculations utilised the analytical solution of the widely-accepted Percus-Yevick 'hard sphere' potential *(15)* and support our earlier experimental findings as described in the main paper.

3. Tables

Table SI-1. Chemical Analysis of the Wastewater.

Determinand	This study	Typical untreated domestic wastewater [a] 'Low' strength	'Medium' strength	'High' Strength
Total Suspended Solids (mg L^{-1})	293	120	210	400
Total Nitrogen (mg-N L^{-1})	37	20	40	70
Phosphorus (mg-P L^{-1})	7.2	4	7	12
Biochemical Oxygen Demand, 5-d 20^{o}C (mg L^{-1})	200 [b]	110	190	350
Boron (μg L^{-1})	194 [c]	121 [d]	NA	NA

Key: NA = not available; (a) Reference *16*; (b) Estimated concentration, based on other measured determinand values, which indicate that the raw wastewater used for this study corresponds with the 'medium' strength wastewater; (c) Boron (B) is widely used as a tracer of detergents in wastewater (it being derived from perborates used in laundry detergents (*17)*) and is used here as a proxy to compare general levels of surfactant contamination. The average B concentration for samples collected across diurnal cycles in July 2008 at this Water Treatment Works was 195 μg L^{-1} (concentrations ranged from 193 μg L^{-1} at low influent flow to 201 μg L^{-1} at peak influent flow). The wastewater sample used for this study was therefore highly representative of the average levels of laundry detergent/surfactant contamination for wastewater at this Works; (d) Average B concentration from wastewater samples collected from a smaller Wastewater Treatment Works, also in South East England but serving 6890 population equivalents. This shows good comparability with the wastewater used in this study in terms of levels of laundry detergent/surfactant contamination. The wastewater used in this study has a slightly higher boron concentration, probably as a result of the greater urban population.

Table SI-2. Representative Particle Size Data. From multi-angle static light scattering.

Angle	q²[1/m²]	CR[kHz]	dCR[%]	Imon	dImon[%]	T[K]	dT[%]	Kc/R	dKc/R[%]	Rad[nm]	dRad[%]
30	4.69E+13	2034.47	5.54	523422	0.05	294.7	0	1.46E-07	5.49	42.26	3.89
40	8.18E+13	1656.04	4.29	523934	0.12	294.7	0	1.40E-07	4.17	48.14	4.74
50	1.25E+14	1388.40	2.48	523742	0.16	294.7	0	1.40E-07	2.32	52.47	2.25
60	1.75E+14	1218.49	0.94	524032	0.06	294.7	0	1.41E-07	0.88	54.47	1.77
70	2.30E+14	1108.27	0.49	523681	0.06	294.7	0	1.40E-07	0.43	53.91	3.90
80	2.89E+14	1029.95	1.82	523936	0.19	294.7	0	1.45E-07	1.63	52.14	3.88
90	3.50E+14	985.25	1.52	522646	0.06	294.7	0	1.48E-07	1.46	53.22	2.71
100	4.11E+14	974.80	0.39	524018	0.08	294.7	0	1.52E-07	0.30	53.02	2.91
110	4.70E+14	984.57	1.88	523340	0.07	294.7	0	1.57E-07	1.81	53.80	4.22
120	5.25E+14	1038.38	0.82	523478	0.07	294.7	0	1.60E-07	0.75	53.75	1.35
130	5.75E+14	1148.16	0.34	523119	0.03	294.7	0	1.64E-07	0.31	53.87	4.08
140	6.18E+14	1340.66	0.79	522766	0.18	294.7	0	1.68E-07	0.62	52.68	1.72
150	6.53E+14	1641.04	0.92	522969	0.01	294.7	0	1.80E-07	0.92	48.86	0.18

Key: q (similar to Q in the SANS experiments) is the modulus of the scattering vector, CR is the count rate, Imon is the total monitor count, T is the absolute temperature of the measurements, Kc/R is the optical constant, and Rad is the particle radius.

4. Settling Velocity

The settling (or terminal) velocity v_s of a spherical object of radius R and density δ_p (= 2.8 g cm^{-3} for our SiO_2NPs) falling under gravity through a fluid of viscosity η and density δ_f is given by Stokes expression *(18)*

$$\upsilon_s = \frac{2}{9} \cdot \frac{(\delta_p - \delta_f)}{\eta} \cdot g \cdot R^2 \qquad \text{(SI-10)}$$

where g is the acceleration due to gravity (980.67 cm s^{-2}). For water at 25 °C, δ_f = 0.998 g cm^{-3} and η = 0.01 g cm^{-1} s^{-1}.

5. Calculation of Surfactant Coverage

The amount of adsorbed surfactant Γ has been estimated in two ways: 1) by a direct calculation using the known concentrations of nanoparticles and surfactant present and, 2) from the experimentally determined layer thickness, using:

1) $$\Gamma = \frac{1000 \,.\, c \,.\, R}{3 \,.\, \Phi \,.\, M_w} \ \mu\text{mol m}^{-2} \qquad \text{(SI-11)}$$

where c is the surfactant concentration (0.0001 g cm^{-3}), R is the particle radius (28 nm), Φ is the dispersion volume fraction (0.0009) and, M_w is the formula weight of the surfactant (1227 g mol^{-1}).

2) $$\Gamma = \frac{1000 \,.\, t \,.\, (\rho_{H2O} - \rho_{shell})}{N_{Av} \,.\, V_{mol} \,.\, (\rho_{H2O} - \rho_{surfactant})} \ \mu\text{mol m}^{-2} \qquad \text{(SI-12)}$$

where t is the adsorbed layer thickness (2.5 nm = (61-56 nm)/2, see Table 1 in main text), V_{mol} is molecular volume (1.85×10^{-21} cm^3 $molecule^{-1}$) and $\rho_{surfactant}$ is the neutron scattering length density ($+0.6\times10^{10}$ cm^{-2}) of the surfactant. ρ_{shell} can either be estimated from a linear combination of ρ_{H2O} and $\rho_{surfactant}$ by making some assumption about the degree of coverage, or included as an adjustable parameter in the model-fitting. The Brij™ surfactants used in Reference 4 below formed adsorbed layers with a surfactant volume fraction of about 80%, but we believe that the much bulkier headgroup of Tween™ would lead to somewhat lower values.

References

1. van Ewijk, G. A., Vroege, G. J. & Philipse, A. P. Convenient preparation methods for magnetic colloids. *J. Magnetism Mag. Mat.* **1999**, *201*, 31-33.

2. Bumb, A., Brechbiel, M.W., Choyke, P.L., Fugger, L., Eggeman, A., Prabhakaran, D., Hutchinson, J., Dobson, P.J. Synthesis and characterization of ultra-small superparamagnetic iron oxide nanoparticles thinly coated with silica. *Nanotechnology*. **2008**, *19*, 335601-335607.

3. Chunhee K., Hsieh, Y.L. Wetting and absorbency of nonionic surfactant solutions on cotton fabrics. *Coll. Surf. A* **2001**, *187*, 385–397.

4. McDermott, D.C., Lu, J.R., Lee, E.M., Thomas, R.K., Rennie, A.R. Study of the adsorption from aqueous solution of hexaethylene glycol monododecyl ether on silica substrates using the technique of neutron reflection. *Langmuir* **1992**, *8*, 1204-1210.

5. Penfold, J., Staples, E., Tucker, I., Cummins, P. Adsorption of non-ionic surfactants on silica sol particles: The effects of sol type and concentration, surfactant type, concentration, and temperature. *J. Phys. Chem.* **1996**, *100*, 18133-18137. And references therein.

6. Costa, C.A.R., Leite, C.A.P., Galembeck, F. Size dependence of Stöber silica nanoparticle microchemistry. *J. Phys. Chem. B* **2003**, *107*, 4747-4755.

7. Donselaar, L.N., Philipse, A.P. Interactions between silica colloids with magnetite cores: diffusion, sedimentation and light scattering. *J. Coll. Int. Sci*. **1999**, *212*, 14–23.

8. www.isis.rl.ac.uk

9. King, S.M., Heenan, R.K. Using COLETTE. *RAL Report RAL-95-005*. Rutherford Appleton Laboratory. **1995**.

10. Wignall, G.D., Bates, F.S. Absolute calibration of small-angle neutron scattering data. *J. Appl. Cryst.* **1987**, *20*, 28-40.

11. Kotlarchyk, M., Chen, S.-H. Analysis of small-angle neutron scattering spectra from polydisperse interacting colloids. *J. Chem. Phys.* **1983**, *79*, 2461-2469.

12. Mildner, D.F.R., Hall, P.J. Small-angle scattering from porous solids with fractal geometry. *J. Phys. D Appl. Phys*. **1986**, *19*, 1535-1545.

13. Triolo, F. *et al*. Fractal approach in petrology: combining ultra small angle, small angle and intermediate angle neutron scattering. *J. Appl. Cryst.* **2000**, *33*, 863-866.

14. Pfeifer, P. Multiple scattering of waves in random media and random rough surfaces. Proceedings of the International Symposium held at Pennsylvania State University 29 July-2 August 1985. Varadan, V., Varadan, V.K. (editors). Pennsylvania State University. **1987**.

15. Ashcroft, N.W., Lekner, J. Structure and resistivity of liquid metals. *Phys. Rev*. **1966**, 145 83-90.

16. Tchobanoglous, G., Burton, F.L., Stensel, H.D. **2003**. Wastewater Engineering: Treatment and Reuse. 4th Edition. Metcalf & Eddy Inc., New York, McGraw-Hill.

17. Holt, M.S., Fox, K.K., Burford, M., Daniel, M., Buckland, H. UK Monitoring study on the removal of linear alkylbenzene sulphonate in trickling filter type sewage treatment plants. Contribution to GREAT-ER Project #2. *Science of the Total Environment* **1998,** *210/211*, 255-269.

18. Lamb, H. Hydrodynamics. 6th Edition. Cambridge University Press. 1932. Reprinted **2006**.